Atmos. Chem. Phys., 9, 9433–9447, 2009
www.atmos-chem-phys.net/9/9433/2009/

Atmospheric Chemistry and Physics

$H_2^{16}O$ and HDO measurements with IASI/MetOp

H. Herbin[1,*], D. Hurtmans[1], C. Clerbaux[2,1], L. Clarisse[1,], and P.-F. Coheur[1,**]**

[1]Spectroscopie de l'Atmosphère, Service de Chimie Quantique et de Photophysique, Université Libre de Bruxelles, Brussels, Belgium
[2]UPMC Univ. Paris 06; Université Versailles St-Quentin; CNRS/INSU, LATMOS-IPSL, Paris, France
[*]now at: Laboratoire d'Optique Atmosphérique, Université des Sciences et Technologies de Lille, 59655 Villeneuve d'Ascq cedex, France
[**]respectively Research Associate and Scientific Research Worker with the F. N. R. S., Belgium

Received: 19 February 2009 – Published in Atmos. Chem. Phys. Discuss.: 8 April 2009
Revised: 19 November 2009 – Accepted: 25 November 2009 – Published: 15 December 2009

Abstract. In this paper we analyze distributions of water vapour isotopologues in the troposphere using infrared spectra recorded by the Infrared Atmospheric Sounding Interferometer (IASI), which operates onboard the Metop satellite in nadir geometry. The simultaneous uncorrelated retrievals of $H_2^{16}O$ and HDO are performed on radiance measurements using a line-by-line radiative transfer model and an inversion procedure based on the Optimal Estimation Method (OEM). The characterizations of the retrieved products in terms of vertical sensitivity and error budgets show that IASI measurements contain up to 6 independent pieces of information on the vertical distribution of $H_2^{16}O$ and up to 3.5 for HDO from the surface up to the upper troposphere (0–20 km). Although the purpose of the paper is not validation, a restricted comparison with sonde measurements shows that the retrieved $H_2^{16}O$ profiles capture the seasonal/latitudinal variations of the water content, with good accuracy in the lowest layer but with larger uncertainties higher in the free and upper troposphere. Our results then demonstrate the ability of the IASI instrument to monitor atmospheric isotopologic water vapour distributions and to provide information on the partitioning of HDO as compared to $H_2^{16}O$. The derivation of the δ_D is challenging and associated with large errors in the uncorrelated retrieval approach chosen here. As a result averaging on the vertical to produce a column-averaged δ_D is required to produce meaningful results for geophysical interpretation. As a case study, we analyse concentration distributions and spatio-temporal variations of $H_2^{16}O$ and δ_D during the October 2007 Krosa super-typhoon over South-East Asia. We show that individual δ_D have uncertainties of 37‰for the vertically averaged values. Using the latter, we suggest that the typhoon produces a so-called amount-effect, where the δ_D is negatively correlated to the water amounts as a result of intense depletion of the deuterated species.

Correspondence to: H. Herbin
(herve.herbin@univ-lille1.fr)

1 Introduction

Water vapour is the most important atmospheric trace gas and a key compound of the global climate (Ciais et al., 2004; Gedzelman et al., 2003; Hartmann, 2002; Lawrence et al., 2002; Smith, 1992). It plays an important role in many atmospheric processes, such as radiative transfer, circulation dynamics (Strong et al., 2007; Hanisco et al., 2007; Kuang et al., 2003; Johnson et al., 2001; Moyer et al., 1996), stratospheric chemistry (Steinwagner et al., 2007; Rosenlof et al., 2001, 2003; McCarthy et al., 2004; Franz et al., 2005; Coffey et al., 2006), cloud formation (Schmidt et al., 2005), precipitation (Bowen and Revenaugh, 2003) and the greenhouse effect (Schneider et al., 1999; Hartmann, 2002). For all of these processes it is important to answer questions such as: What is the distribution of moisture sources and sinks? What are the distributions of moist processes controlling the hydrology cycle? The analysis of the water vapour isotopologic partitioning, which is strongly influenced by evaporation sources and condensation conditions, is useful to derive information on the water vapour sources, sinks and dynamics (Zahn et al., 2006).

Published by Copernicus Publications on behalf of the European Geosciences Union.

Table 1. Some specifications of TES and IASI instruments.

	TES	IASI
Spectral coverage	650–2250 cm^{-1}	645–2760 cm^{-1}
Spectral resolution (apodized)	0.1 cm^{-1} (nadir mode)	0.5 cm^{-1}
Signal to noise ratio	600	500–1000
Field of view	5.3×8.4 km (nadir mode)	12km diameter pixels recorded simultaneously in a 2×2 matrix.

There are several stable isotopologic species of the water molecule ($H_2^{16}O$, $H_2^{18}O$, $H_2^{17}O$ and HDO being the most abundant), each with different vapour pressures and reaction rates. The isotopic composition is given in per mil (‰) units using the conventional δ notation relative to the V-SMOW standard, where $\delta=\left(\frac{R}{R_{\mathrm{SMOW}}}-1\right)\times 1000$, and R denotes the isotopologic mass ratio, with R_{SMOW}=[HDO]/[$H_2^{16}O$]=0.31152×10^{-3}. Although water isotopologue measurements have been successfully used in e.g. upper troposphere lower stratosphere exchange (Moyer et al., 1996; Johnson et al., 2001; Webster and Heymsfield, 2003) and subtropical troposphere dynamics (Worden et al., 2007; Galewsky et al., 2007), there are few measured profiles of the heavier isotopologues (Zahn et al., 2006, and references therein). Especially satellite observations, which can offer distributions over large regions, are missing.

In a previous paper, we have demonstrated the ability of space-borne infrared sounders to measure simultaneously the vertical profiles of the main water isotopologues (i.e. $H_2^{16}O$, $H_2^{18}O$ and HDO) (Herbin et al., 2007). These results were obtained using the infrared spectra recorded by the Interferometric Monitor for Greenhouse gases (IMG) instrument. Likewise, distributions of the tropospheric HDO/$H_2^{16}O$ ratio were reported using measurements from the Tropospheric Emission Spectrometer (TES) (Worden et al., 2006, 2007). The HDO/$H_2^{16}O$ ratios derived from TES have been applied to improve understanding of the characteristics of hydrologic budgets in monsoonal regions (Brown et al., 2008). IASI is an operational meteorological instrument onboard the European MetOp-A platform, which targets primarily temperature and water vapour profile measurements in the troposphere (Clerbaux et al., 2007, 2009; Schlüssel et al., 2005). As TES, IASI is a Fourier transform spectrometer; some specifications of the two sounders (Beer et al., 2001; Schlüssel et al., 2005) are summarized in Table 1. Despite a coarser spectral resolution as compared to TES, IASI is expected to provide accurate water vapour measurements because of a very high signal to noise ratio. IASI has further the advantage over TES of spatial coverage and temporal sampling and of covering the shortwave part of the thermal infrared above 2500 cm^{-1}, which contains strong HDO lines.

Here, we present the first simultaneous uncorrelated retrievals of $H_2^{16}O$ and HDO vertical distributions from IASI. The goal of this preliminary study is to characterize the capabilities of the IASI in providing information on concentration distributions of $H_2^{16}O$, HDO but also on the more challenging δ_D.

In the next section, we describe briefly the IASI instrument, the measured radiance spectra and the retrieval method. Section 3 presents tropospheric vertical distributions for a selection of IASI spectra coincident with data from radiosondes (Gaffen, 1994) and representative for different latitudes and seasons. The retrieved profiles are discussed with respect to the error budgets and the vertical sensitivity of the measurements. We also examine in this section the advantage of using, for the HDO retrievals, the reflected solar part of the spectrum for the inversion process. In Sect. 4 we use the unprecedented spatial and temporal sampling of IASI to probe the regional isotopologic composition of water vapour during a major meteorological event (Krosa Typhoon in early October 2007) and discuss the capabilities of the instrument to capture δ_D variations, which can be useful for the monitoring of our environment. Section 5 summarizes our results and presents perspectives on future applications.

2 Measurements and methods

2.1 Measurements

IASI is one of the eleven instruments launched onboard the polar sun-synchronous orbiting Metop-A platform on 19 October 2006. The IASI instrument (Clerbaux et al, 2007, 2009; Schlüssel et al., 2005) is a nadir-viewing Fourier transform interferometer which records the thermal infrared emission of the Earth-atmosphere system between 645 and 2760 cm^{-1} with an apodized spectral resolution of 0.5 cm^{-1}. IASI's field of view corresponds to a 2×2 pixel matrix where at nadir each pixel has a 12 km footprint on the ground. Its ability to scan across a swath of 2200 km allows for global coverage twice a day with a good horizontal resolution. The IASI specifications are ideal for studying the atmosphere from a local to a global scale. The main purpose of the IASI mission is to provide temperature and tropospheric water vapour profiles with 1 K, 10–15% accuracies and with 1 and 2 km

vertical resolutions respectively (Clerbaux et al., 2007, 2009; Schlüssel et al., 2005).

The $H_2^{16}O$ and HDO profiles are retrieved from the IASI spectra using the *Atmosphit* software developed at the Université Libre de Bruxelles. This software is based on a detailed line-by-line radiative transfer model, including ray tracing for various geometries and a retrieval scheme relying on the Optimal Estimation Method (OEM) (Rodgers, 2000). The theoretical elements relevant for the present study are similar to those described by Barret et al. (2005), and Coheur et al. (2005). They are only briefly summarized hereafter.

2.2 Retrieval methodology

For an atmosphere divided in discrete layers, the forward radiative transfer equation gives an analytical relationship between the measured vector $\boldsymbol{y}$ (in our case, the radiance) and the true atmospheric state $\boldsymbol{x}$ (e.g. variables to be retrieved: surface temperature, vertical concentration profile) and is written as:

$$\boldsymbol{y}=\boldsymbol{F}(\boldsymbol{x};\boldsymbol{b})+\boldsymbol{\varepsilon} \tag{1}$$

where $\boldsymbol{F}$ is the forward radiative transfer function, $\boldsymbol{b}$ represents the fixed parameters affecting the measurement (e.g. atmospheric temperature, pressure, instrumental line shape (ILS)) and $\boldsymbol{\varepsilon}$ is the measurement noise.

The radiative transfer function is computed using the line parameters (positions, intensities, broadening, shifting and their temperature dependency) and absorption cross-sections compiled in spectroscopic databases, as well as the absorption continua from the MT-KD model (Clough et al., 2005). The molecular absorption lines are computed using a Voigt line shape and the resulting spectrum is processed to account for the ILS contribution. The latter is represented by a Gaussian function with $0.5\,\mathrm{cm}^{-1}$ full width at half maximum and set on a $0.25\,\mathrm{cm}^{-1}$ spectral sampling grid.

The retrieval method aims at determining the state vector $\boldsymbol{x}$ from the measurement vector $\boldsymbol{y}$. For nadir-viewing satellites, however, the spectra provide an integrated view of the atmosphere. As a consequence, the retrieval of a vertically resolved profile from the measurement is mathematically ill conditioned, meaning that it has no unique solution. A meaningful solution can, however, be obtained by regularizing the retrieval with a priori information about the variables. This information is composed of an a priori profile $\boldsymbol{x}_a$ and an a priori variance-covariance matrix $\boldsymbol{S}_a$ (Rodgers, 2000). In this case, the goal of the inversion is to find $\hat{\boldsymbol{x}}$, which is the approximation of the true state $\boldsymbol{x}$, which best agrees with both the measurement and the a priori information. The solution $\hat{\boldsymbol{x}}$ is found by iterating:

$$\hat{\boldsymbol{x}}_{i+1}=\boldsymbol{x}_a+(\mathbf{K}_i^T\boldsymbol{S}_\varepsilon^{-1}\mathbf{K}_i^T+\boldsymbol{S}_a^{-1})^{-1}\mathbf{K}_i^T\boldsymbol{S}_\varepsilon^{-1} \left[\boldsymbol{y}-\boldsymbol{F}(\hat{x}_i)+\mathbf{K}_i(\hat{\boldsymbol{x}}_i-\boldsymbol{x}_a)\right] \tag{2}$$

and the error covariance is given by:

$$\hat{\boldsymbol{S}}_{i+1}=(\mathbf{K}_{i+1}^T\boldsymbol{S}_\varepsilon^{-1}\mathbf{K}_{i+1}+\boldsymbol{S}_a^{-1})^{-1} \tag{3}$$

with $\mathbf{K}_i$ being the Jacobian matrix, the rows of which are the partial derivatives of the measurement with respect to the retrieved variables: $\mathbf{K}_i=(\partial\boldsymbol{F}/\partial\boldsymbol{x})_i$, and $\mathbf{K}^T$ is its transpose. $\boldsymbol{S}_\varepsilon$ is the measured signal error variance-covariance matrix and is chosen to be diagonal, $\boldsymbol{S}_\varepsilon=\sigma_\varepsilon^2\boldsymbol{I}$ (Barret et al., 2005; Coheur et al., 2005), where σ_ε is a constraint representing the noise equivalent spectral radiance. The retrieved state is obtained after convergence, when the absolute difference between every element of $\boldsymbol{F}$ modeled at two successive iteration steps, $\left|\boldsymbol{F}(\hat{x}_{i+1})-\boldsymbol{F}(\hat{x}_i)\right|$, is less than a fraction (20%) of σ_ε.

The characterization of the retrieved quantities in terms of sensitivity and error sources is essential to estimate the quality of the results. In the case of the linear approximation used here, the OEM provides an efficient way for characterizing the retrieved state, which is given by Rodgers, (2000):

$$\hat{\boldsymbol{x}}=\boldsymbol{x}_a+\boldsymbol{A}(\boldsymbol{x}-\boldsymbol{x}_a)+\boldsymbol{G}(\boldsymbol{\varepsilon}+\boldsymbol{K}_b(\boldsymbol{b}-\hat{\boldsymbol{b}})), \tag{4}$$

where $\hat{\boldsymbol{b}}$ is the approximate of the model parameters $\boldsymbol{b}$, the Jacobian $\boldsymbol{K}_b=\partial\boldsymbol{F}/\partial\boldsymbol{b}$ characterizes the sensitivity of the forward model $\boldsymbol{F}$ to the model parameters. $\boldsymbol{G}$ is the gain matrix whose rows are the derivatives of the retrieved state with respect to the spectral points and it is defined by:

$$\boldsymbol{G}=\partial\hat{\boldsymbol{x}}/\partial\boldsymbol{y} \tag{5}$$

$\boldsymbol{A}$, the averaging kernel matrix, gives a measure of the sensitivity of the retrieved state to the true state. It is defined by:

$$\boldsymbol{A}=\partial\hat{\boldsymbol{x}}/\partial\boldsymbol{x}=\boldsymbol{G}K \tag{6}$$

At a given level, the peak of the averaging kernel row gives the altitude of maximum sensitivity whereas its full width at half maximum is an estimate of the vertical resolution. The trace of $\boldsymbol{A}$, known as the Degrees Of Freedom for Signal (DOFS), indicates the number of independent values of the state vector which can be retrieved from the measurements.

The global error can be inferred from Eq. (3) by considering the difference between the retrieved and the true state:

$$\hat{\boldsymbol{x}}-\boldsymbol{x}=(\boldsymbol{A}-\boldsymbol{I})(\boldsymbol{x}-\boldsymbol{x}_a)+\boldsymbol{G}\varepsilon+\boldsymbol{G}K_b(\boldsymbol{b}-\hat{b}) \tag{7}$$

In this Eq. (6), the first term $[(\boldsymbol{A}-\boldsymbol{I})(\boldsymbol{x}-\boldsymbol{x}_a)]$ is the smoothing error, which accounts for the vertical sensitivity of the measurements to the retrieved profile; the second term $[\boldsymbol{G}\varepsilon]$ is the measurement error, associated to the spectral noise; and the third one $[\boldsymbol{G}K_b(\boldsymbol{b}-\hat{\boldsymbol{b}})]$ is the model parameters error, which represents the imperfect knowledge of the model parameters.

Their covariance matrices are respectively given by:

$$\boldsymbol{S}_{\text{smoothing}}=(\boldsymbol{A}-\boldsymbol{I})\boldsymbol{S}_a(\boldsymbol{A}-\boldsymbol{I})^T \tag{8}$$

$$\boldsymbol{S}_{\text{meas.}}=\boldsymbol{G}\boldsymbol{S}_\varepsilon\boldsymbol{G}^T \tag{9}$$

$$\boldsymbol{S}_{\text{mod. param.}}=\boldsymbol{G}K_b\boldsymbol{S}_b(\boldsymbol{G}K_b)^T \tag{10}$$

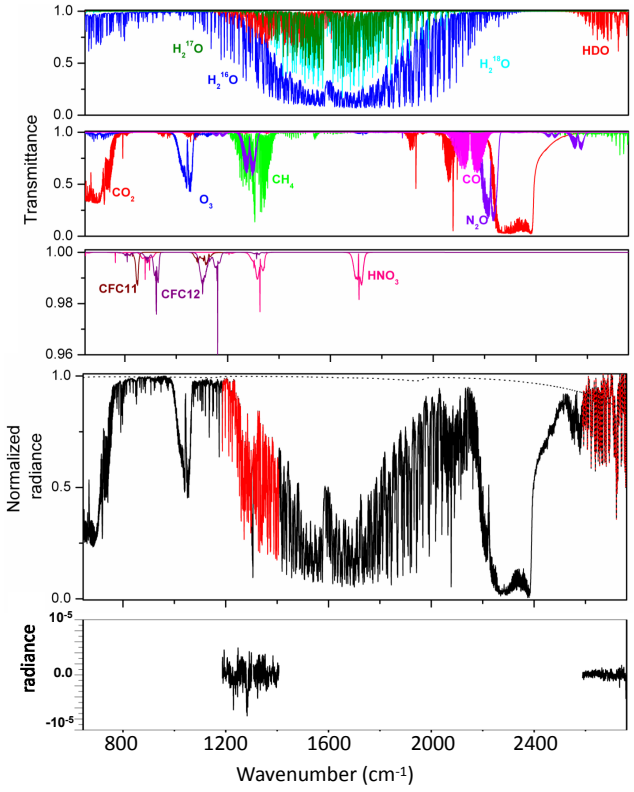

Fig. 1. Retrieval spectral windows. Top: $H_2^{16}O$ (blue), $H_2^{17}O$ (green), $H_2^{18}O$ (cyan), HDO (Red) and other trace gases (lower panel) transmittance spectra. Middle: IASI measured spectrum (normalized radiance, in black) and fitted spectrum (red) in the spectral windows used for retrieving $H_2^{16}O$ and HDO profiles. The average IASI noise is indicated by a black dashed line. Bottom: The last black lines show the residual (observed-calculated) spectra.

with $\boldsymbol{S}_b$ representing uncertainty on the forward model parameters. The latter includes the impact of interfering species, which are simultaneously fitted, as well as the uncertainty on the air temperature profile (uncorrelated uncertainty of 1 K on each retrieved level). Here, the line parameters error is not considered.

The total error variance-covariance matrix can then be regarded as the sum of these individual contributions:

$$\boldsymbol{S}_{\text{total}} = \boldsymbol{S}_{\text{smoothing}} + \boldsymbol{S}_{\text{meas}} + \boldsymbol{S}_{\text{mod. param.}} \quad (11)$$

2.3 Data analysis

For the retrievals, the water vapour a priori covariance matrices $\boldsymbol{S}_a$ and the a priori state vector $\boldsymbol{x}_a$ are built based on local radiosondes data over 2 months (day and night) and averaged on 5 different latitudinal bands (+90°, +60°), (+60°, +23°), (+23°, −23°), (−23°, −60°) and (−60°, −90°). This thus results in a set of five different prior information, representative of a given latitude band, but with for each a rather large variability representing spatial and temporal variations within the two month period considered. This method allows on one hand – using a latitudinal dependent $\boldsymbol{x}_a$ – to start the retrieval with reasonable water concentrations and on the other hand – using a large variability – to minimize the impact of the prior in the retrieved profiles (Herbin et al., 2007). The a priori information covers altitudes ranging from the ground up to 20 km, interpolated on a grid of 2 km. The a priori constraint vector and covariance matrices for HDO are identical to those of $H_2^{16}O$, multiplied, however, by the standard isotopologic ratio and corrected by Rayleigh distillation model. The spectroscopic parameters were extracted from the HITRAN 2004 database (Rothman et al., 2005). Because the signal to noise ratio varies over the IASI spectra (see Fig. 1), we use for the retrievals a value of σ_ε of the order of the expected IASI noise and close to the Root Mean Squares (RMS) of typical retrievals, ie. $\sigma_\varepsilon = 2\times10^{-6}$ W/(cm^2 sr m^{-1}).

Water vapour isotopologues absorb almost everywhere in the spectral range of IASI, with many strong lines that saturate the absorption signal throughout the ν_2 and (Fig. 1). We have selected two spectral windows for the simultaneous retrieval of $H_2^{16}O$ and HDO, extending respectively from 1186.95 to 1300.75 and 1307.25 to 1406.40 cm^{-1} (thus removing the strong methane Q-branch of ν_4 and), located both on the long wavelength end of the ν_2 band. IASI spectra cover also parts of the infrared above 2500 cm^{-1}, where the upwelling source function during daytime is dominated by the reflected solar radiation. Absorption of this radiation is mainly attributable to methane (CH_4) and HDO. It therefore offers a potential improvement on the sensitivity of IASI to these species in the lowest layers of the atmosphere (see e.g. Razavi et al., 2009). To analyze this for HDO, we have used a supplemental spectral window extending from 2588.00 to 2757.30 cm^{-1}. For the sake of illustration, Fig. 1 gives an example of a spectral fit in the selected windows, showing also the typical quality of the residual spectra (Observed-Calculated).

The retrievals use along with the water vapour a priori constrain specified above, the level 2 pressure and temperature profiles from the operational processing at Eumetsat. In the inversion step, the volume mixing ratios (vmr) for water isotopologues are retrieved on 10 discrete vertical layers, extending from the ground up to 20 km as 0–1, 1–3, 3–5, 5–7, 7–9, 9–11, 11–13, 13–15, 15–17 and 17–20 km. In the spectral range used, the surface temperature, the strength of reflected solar radiation ("reflectivity"), the total columns of $H_2^{17}O$, CO_2, N_2O, CH_4 and HNO_3, and the profiles of $H_2^{16}O$, HDO and $H_2^{18}O$ are adjusted simultaneously but importantly without a priori correlation between the different isotopologues. This uncorrelated approach differs from that used in other studies (Worden et al., 2006; Schneider et al., 2006). This allows for a detailed characterization of the extent of information contained in the IASI measurements for the two species independently but produces large errors on the δ_D value (see Sect. 3).

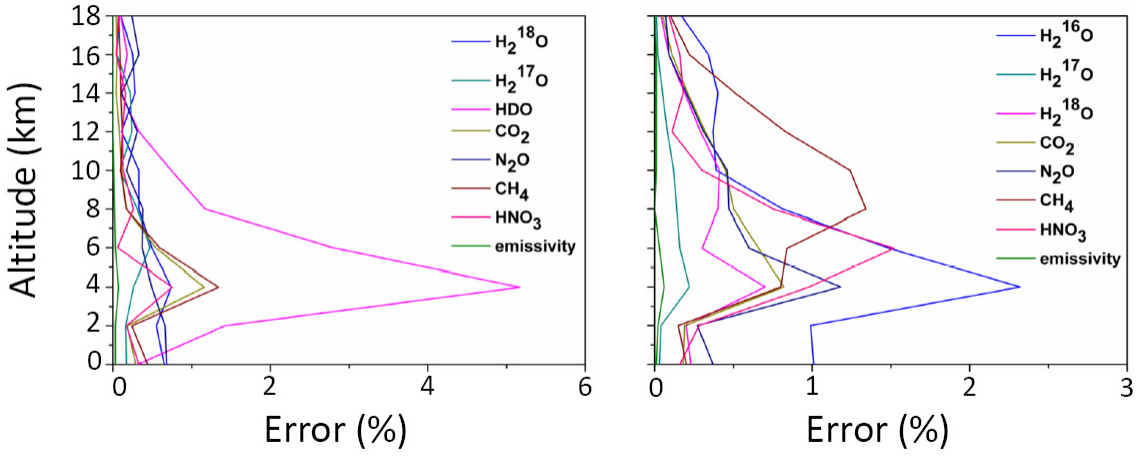

Fig. 2. Error profiles of interfering species and emissivity for $H_2^{16}O$ (left) and HDO (right) retrieval.

3 Retrievals and characterization

The goal of this section is to characterize the capabilities of IASI to obtain vertically resolved profiles of $H_2^{16}O$ and HDO from the ground up to the upper troposphere/lower stratosphere region. At first it should be pointed out that interferences have only minor impact on the retrievals. To illustrate this, Fig. 2 gathers the errors due to interfering species and the emissivity for the $H_2^{16}O$ (left panel) and HDO (right panel) retrievals. It shows that these parameters account for less than 1% in the total error; they are not included further in the discussion. In fact Fig. 2 shows that in addition to the smoothing and measurements error, the most influent parameter in the error budget will for the $H_2^{16}O$ retrieval be HDO determination and reciprocally.

3.1 Information from the shortwave window

In order to quantify the benefit of the shortwave retrieval window above 2500 cm^{-1} for the HDO profile, we have performed a series of retrievals on IASI spectra significantly affected by the reflection of the solar radiation. Figure 3 shows an example of HDO error budgets and averaging kernels resulting from the inversion of a IASI observation at Southern mid-latitude above the ocean, in December 2007, performed without (upper panel) and with (lower panel) the supplemental shortwave window. The χ^2 and RMS are slightly better for the spectral fit when the shortwave is considered. For the RMS, this results from the fact that the spectral fit is better in the shortwave where the lines are less saturated (even though the measurement noise is larger). With regard to the χ^2, it is also better for the combination and this is explained by the weaker signal to noise ratio in the spectral window 2588–2757 cm^{-1}, which necessitates to multiply the measurement-noise constrain σ_ε by a factor two; hence convergence is more easily achieved. The degrees of freedom for the signal are respectively 3.01 and 2.61. These highlight mainly the gain of information on HDO close to the surface from using the reflected solar radiation, with the error at ground-level decreasing from 18.5% to 12.9% for the case shown in Fig. 3. Interestingly, the retrieved $H_2^{16}O$ profile is also slightly improved following this procedure. It is worth pointing out that the use of the shortwave window at night, does not degrade the retrieval. Accordingly, and despite that only a small number of IASI spectra show sufficient signal-to-noise above 2500 cm^{-1} to benefit the HDO retrieval, the window was therefore kept in all further analyses.

3.2 Quality assessment of $H_2^{16}O$ and HDO profiles

To make a preliminary assessment of the quality of the water vapour retrievals (no validation is attempted here), we have compared the retrieved profiles to a set of humidity soundings at 6 sites, representative of different latitudes (Table 2) on the same day (1 September 2008). The water vapour radiosonde data have been provided by the Wyoming University. The co-localisation criteria were set on the spatial scale to 1° latitude and 1° longitude from the six stations and on the temporal scale to within twelve hours of the soundings (Tables 2 and 3). The a priori used is that described in Sect. 2.3 and is thus different for the different stations, except for the two tropical ones.

Figure 4a shows the profile comparison between the $H_2^{16}O$ retrievals, the humidity soundings, the IASI level 2 delivered operationally and the a priori profiles. Figure 4b and c show in addition the averaging kernels and the error budgets of the coincident IASI/sonde water vapour measurement of Table 2 as well as the Fig. 4d show the relative difference $[(\boldsymbol{x}_i - \boldsymbol{x}_s) \times 200/(\boldsymbol{x}_i + \boldsymbol{x}_s)]$, $\boldsymbol{x}_i$ being respectively retrieved profile, a priori profile and level 2 profile; $\boldsymbol{x}_s$ are the smoothed water vapour profiles calculated from the measured profiles $\boldsymbol{x}_{\text{sonde}}$ according to Rodgers (2000):

$$\boldsymbol{x}_s = \boldsymbol{x}_a + \boldsymbol{A}(\boldsymbol{x}_{\text{sonde}} - \boldsymbol{x}_a) \quad (12)$$

Table 2. Coincident IASI and water vapour sonde measurements for six locations (identified by name, latitude, longitude) on 1 September 2008. The DOFS for $H_2^{16}O$ and HDO are given at each site. Numbers in parentheses for sun reflectance parameter are the standard deviation in units of the least significant digits.

Observing Site	Latitude, Longitude	Day/Night	Sun "Reflectivity"	$H_2^{16}O$ DOFS	HDO DOFS
Novolazarevskaja	−70.76, 11.82	Day	$5\ 10^{-8}$ (3)	3.80	1.34
Santo Domingo	−33.61, −71.62	Day	$1.5\ 10^{-7}$ (0.3)	5.18	2.88
Darwin	−12.42, 130.88	Night	0	5.86	3.37
Kingston	18.06, −76.84	Day	$1.2\ 10^{-7}$ (0.3)	5.91	3.50
Hailar	49.22, 119.75	Day	$3.0\ 10^{-7}$ (0.3)	5.09	3.03
Bjornoya	74.51, 19.02	Night	0	4.05	2.15

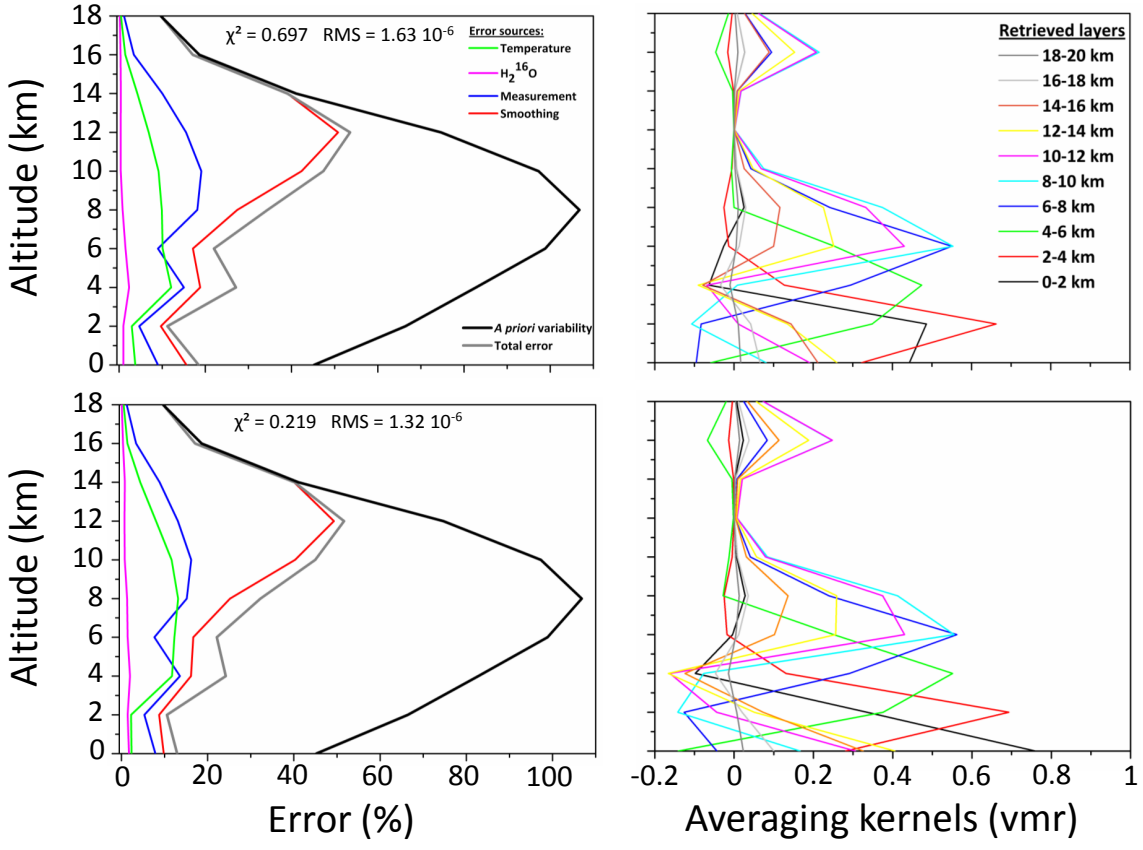

Fig. 3. HDO profile retrieval characterization for a mid-latitude scene with (bottom) and without (top) taking into account the shortwave window in the retrieval procedure. Left: Error profiles. The curves are the square root of the diagonal elements of the *prior* and *posterior* error covariance matrices. The errors due to uncertainties on the temperature profiles are calculated assuming an uncorrelated uncertainty of 1 K. The errors associated with the uncertainties on the others species (i.e. $H_2^{17}O$, $H_2^{18}O$, CH_4, CO_2, N_2O, HNO_3) are negligible and therefore not shown. Right: Averaging kernels, in volume mixing ratio units for the ten retrieved layers. Degrees of freedom for signal are respectively 3.01 and 2.61 with or without the shortwave band taken into account.

This smoothing accounts for the lower vertical resolution of the IASI observing system and thus allows a meaningful comparison with the retrieved profiles. In all cases, we find that the $H_2^{16}O$ retrieved profiles are in reasonable agreement with the sonde values over the entire altitude range but that they provide a significant improvement with respect to the prior latitudinal climatology or the IASI operational L2 product only close to the surface. There the averaged deviation is 11.3% and is in line with the expectation from the mission. In the free troposphere and higher the averaged deviation is

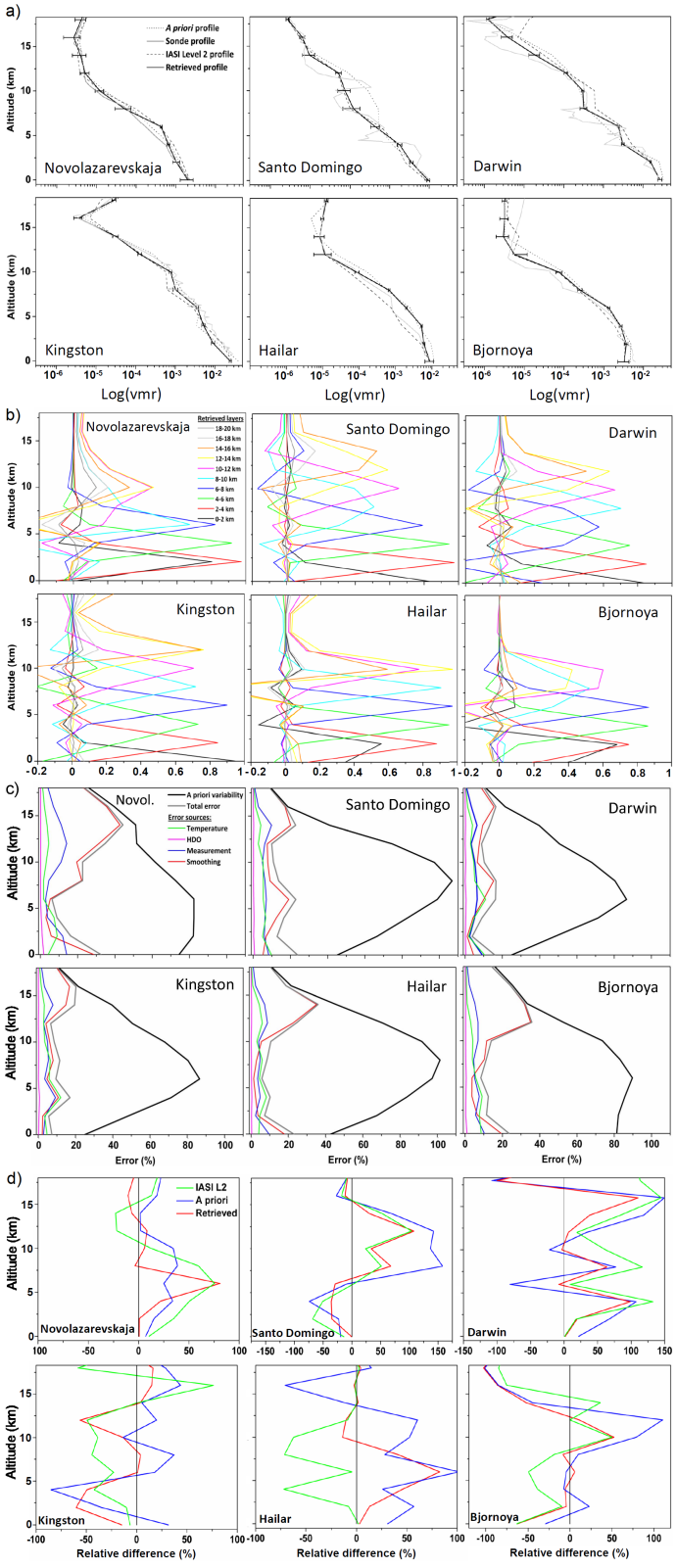

Fig. 4. **(a)** Retrieved $H_2^{16}O$ profiles (vmr) from IASI observations made on 1 September 2008 for six different sites (see Table 2). The grey and black lines represent the sonde and retrieved profiles respectively. The black dashed and dot lines are the a priori and the level 2 IASI profiles respectively. **(b)** Averaging kernels related to (a), in volume mixing ratio units, for each retrieved layers. The corresponding degrees of freedom for signal are reported in Table 2. **(c)** Error profiles related to (a). **(d)** Relative differences (see text). Red, blue and green lines represent respectively the retrieved, a priori and level 2 differences in comparison to the sonde profiles.

Table 3. DOFS of coincident IASI and water vapour sonde measurements above Hawaii (+19.72°, −155.05°) for selected days in September 2008, December 2007, March and June 2008.

Dates	$H_2^{16}O$ DOFS	HDO DOFS
21 September 2008	5.73	3.09
21 December 2007	5.91	3.35
28 March 2008	5.81	3.26
21 June 2008	5.65	3.07

much larger and often has an oscillatory behaviour. This can be partly related to the loose co-location criteria but also suggest the difficulty in capturing small-scale variations in the vertical profile. However, the large latitudinal dependence of the retrieved profiles is adequately captured. For tropical scenes (at Darwin and Kingston), the volume mixing ratios are for instance almost one order of magnitude larger than for the regions with the highest latitude (at Novolazarevskaja and Bjornoya).

The HDO profiles from the same scene have been retrieved starting, as explained above, from a priori profiles constructed from the $H_2^{16}O$ ones, divided by the SMOW ratio and corrected by the Rayleigh distillation model (Zhang et al., 2005). Looking at the general shapes of the profiles, we find that the simultaneous/uncorrelated retrieval produces HDO profiles that have a similar vertical structure as the corresponding $H_2^{16}O$ ones (Fig. 5a). We also suggest that the impact of the prior is relatively small, as apparent from the relative differences in Fig. 5d, which further tend to show the inadequateness of the Rayleigh distillation curve in many cases. These conclusions hold despite weaker vertical sensitivity for the deuterated isotopologue. In fact, the averaging kernels for $H_2^{16}O$ reveal a maximum sensitivity in the tropics and also at mid-latitudes during daytime, with an integrated kernel function spanning the entire altitude range from the surface to 14 km, degrading to 2–12 km at mid-latitudes during night-time. For the highest latitudes there is sensitivity only between 2 and 10 km. For HDO, the measurements are sensitive between the ground level and 12 km for tropical and mid-latitude regions during the day but from 2 and 12 km during the night. At the higher latitudes the sensitivity to HDO is limited to the altitude range between 2 and 8 km. This is further highlighted by the degrees of freedom, listed in the Table 2. It is important to note that whatever the HDO quantity, the constraint is weak enough in order to avoid a major contribution of the a priori (see relative differences graphics of the Fig. 5d).

One result that follows from the above is that the information on the isotopologic ratio, which will be discussed next, is obviously limited by HDO, which has the lowest information content. For each case of Figs. 4a and 5a, the error profile budget is also displayed (see Figs. 4c and 5c). The different curves correspond to the square root of the diagonal elements of the measurement error, the smoothing error and the model parameter error covariance matrices (Herbin et al., 2007). The error analysis confirms that the retrievals are mainly driven by a priori information above 16 km for both isotopologic species. For $H_2^{16}O$, the total error is mostly below 15% over the entire altitude range of the troposphere, increasing to 30% near the surface in the situations where the measurements are less sensitive (highest latitudes). This theoretical total error, which is compliant with the 10% accuracy expected from the mission (Clerbaux et al., 2007, 2009; Schlüssel et al., 2005), is significantly lower than the computed relative differences with sonde data (Fig. 4d). This tends to show the difficulty of achieving in reality this level of accuracy on the profile. The total error is evenly distributed between the temperature, the measurement and the smoothing errors, with additional contributions from uncertainties on model parameters being essentially negligible. For HDO the error on the profile is mainly below 20%, increasing to 40% at the ground level of the highest latitudes, with the smoothing error becoming very dominant. As could be anticipated from the discussion above, the total error is particularly small when the sensitivity is high, with errors reaching, for instance, 7% for $H_2^{16}O$ and 11% for HDO near the surface at Kingston. In all cases and for both isotopologues, the retrieval makes a substantial improvement with respect to the a priori variability. The most significant improvement is in the troposphere between 4 and 8 km, where the a priori uncertainty is largest. To close this sensitivity overview, it is worth noting here the difference in sensitivity between the two tropical locations (Darwin and Kingston) recorded respectively during day and night, which is illustrative for the improvement due to the shortwave retrieval window discussed in Sect. 3.1. It is also worth stressing that the present analysis shows similarities with the results previously obtained from IMG (Herbin et al., 2007). With IASI we do find, however, a higher vertical sensitivity for both isotopologues, likely due to the better signal to noise ratio of the spectra.

Figures 6 and 7 are identical to Figs. 4 and 5 but for observations above a single station (Hawai) on four different days: 21 September 2008, 21 December 2007, 28 March 2008 and 21 June 2008, representatives for the different seasons at tropical locations. Figure 6a shows that the total $H_2^{16}O$ concentrations and the profiles are very similar for the four dates. This is also the case for the DOFS (see Table 3) and error budgets (Fig. 6b and c). At this location, the uncertainty is always below 20% whatever the season or altitude. For HDO, the same remarks can be made. Nevertheless, we can see from the profiles of the Figure 7a that the HDO amount above 10 km is higher in March and June than in September and December. This is corroborated by the sensitivity that is better at high altitudes in March and June (see Fig. 7b). In all cases, the HDO uncertainty at the surface is below 25 % and reaches 40 % over the entire altitude. Therefore, we can

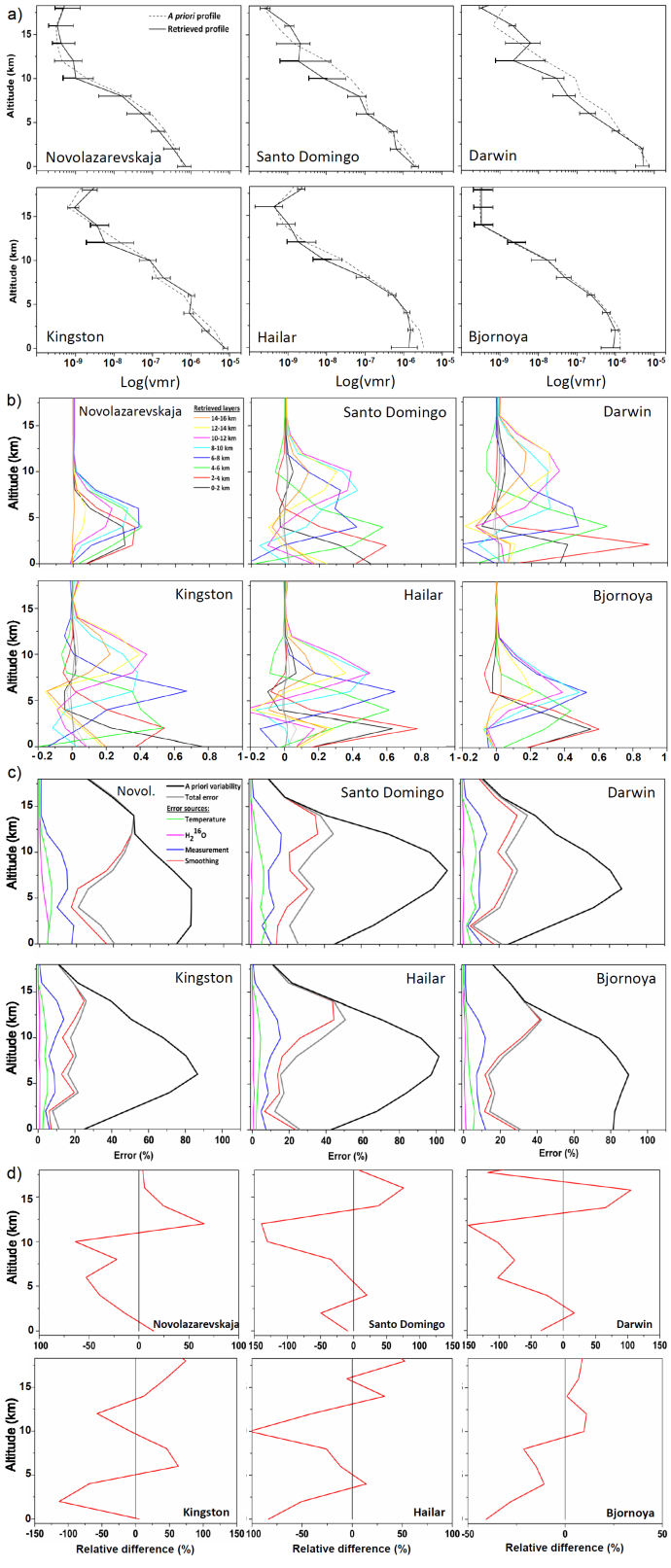

Fig. 5. **(a)** Same as Fig. 4a for HDO. The a priori profiles for HDO have been constructed from those of $H_2^{16}O$ relying on the Rayleigh distillation model (see text for details). **(b)** Averaging kernels related to (a), in volume mixing ratio units, for each retrieved layers. The corresponding degrees of freedom for signal are reported in Table 2. **(c)** Error profiles related to (a). **(d)** Relative difference between retrieved and a priori profiles related to (a).

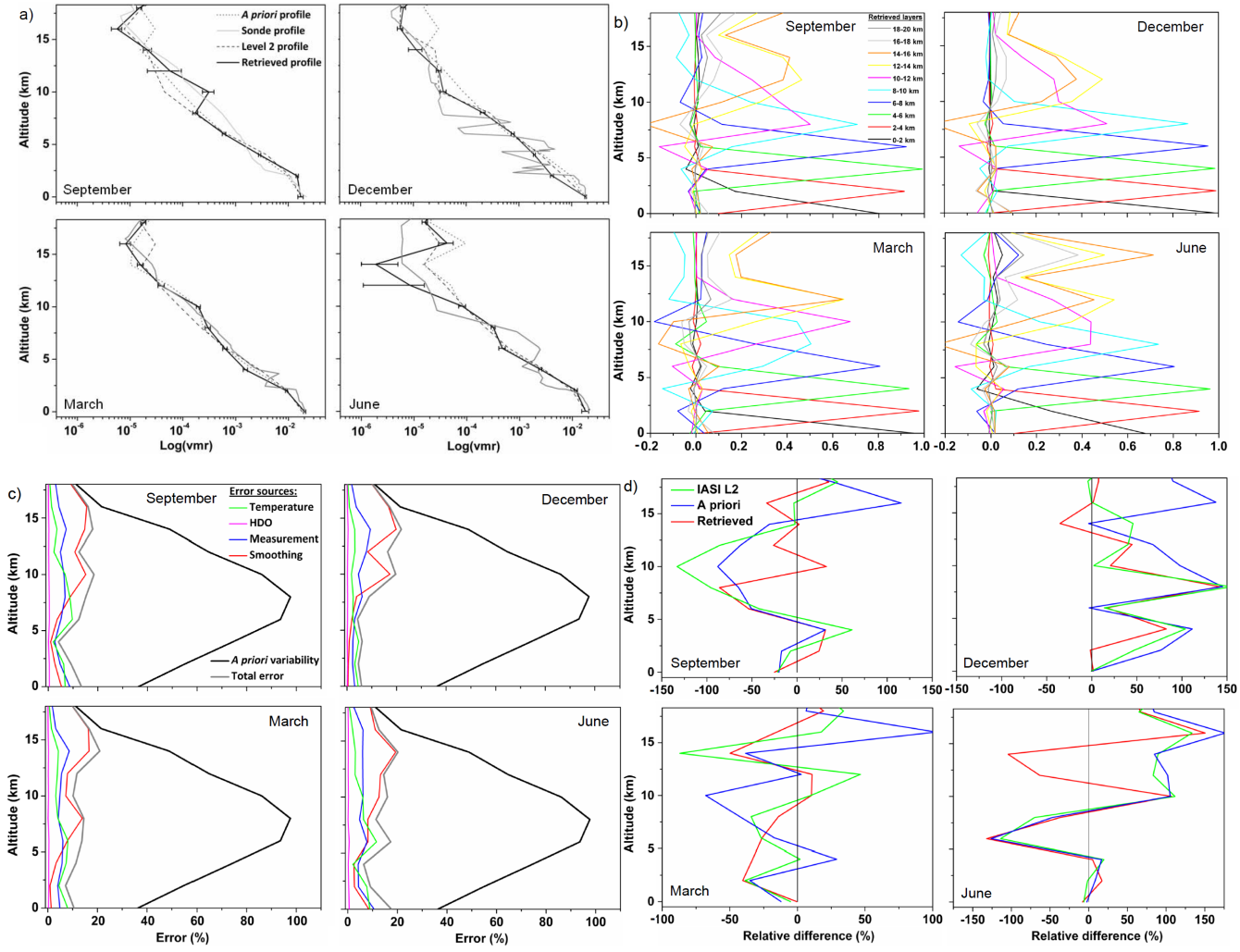

Fig. 6. **(a)** Same as Fig. 4a for $H_2^{16}O$ profiles (vmr) retrieved from IASI observations at Hawaii on four days (top to bottom): 21 September 2008, 21 December 2007, 28 March 2008 and 21 June 2008. **(b)** Averaging kernels related to (a), in volume mixing ratio units, for each retrieved layers. The corresponding degrees of freedom for signal are reported in Table 3. **(c)** Error profiles related to (a). **(d)** Relative difference between retrieved and a priori profiles related to (a).

conclude that the impact of seasons is negligible for tropical scenes where the sensitivity is highest.

3.3 Calculation of δ_D

The profiles of the two isotopologues displayed in Figs. 4, 5, 6 and 7 do not allow, as such, the detection of any unexpected evolution in the isotopologic vertical distribution, which occurs on a finer scale. For this purpose, the calculation of the δ_D values is a prerequisite. Although the quality of the results obtained for each isotopologue demonstrates the capability of IASI to observe isotopologic ratio profiles, the total retrieval errors on each is such that the error on δ_D is rather large. It can be calculated by:

$$\delta\frac{[\mathrm{HDO}]}{[\mathrm{H2O}]} = \frac{\delta[\mathrm{HDO}]}{[\mathrm{H2O}]} - \frac{[\mathrm{HDO}]}{[\mathrm{H2O}]^2}\delta[\mathrm{H2O}] \quad (13)$$

Applied on a typical IASI tropical observation, we calculate uncertainties on δ_D from 96 to 458‰for surface to 20 km levels of the retrieved profile. This is the most pessimistic view recalling, indeed, that the vertical resolution of the latter is of the order of a few kilometres in the best cases. Accordingly, column-averaged δ_D values and uncertainties would be more representative of the measurements. The δ_D errors on the corresponding partial column 0–8 km reduce for instance to 37‰. This value is slightly larger than that obtained from TES analyses (Worden et al., 2006), which uses a constrained method in which the δ_D is retrieved by including correlation between H_2O and HDO from a climate model (δ_D around 12 per mil in the same latitude range). Nevertheless, these errors are still small in comparison to the expected variability (cf. Sect. 4.).

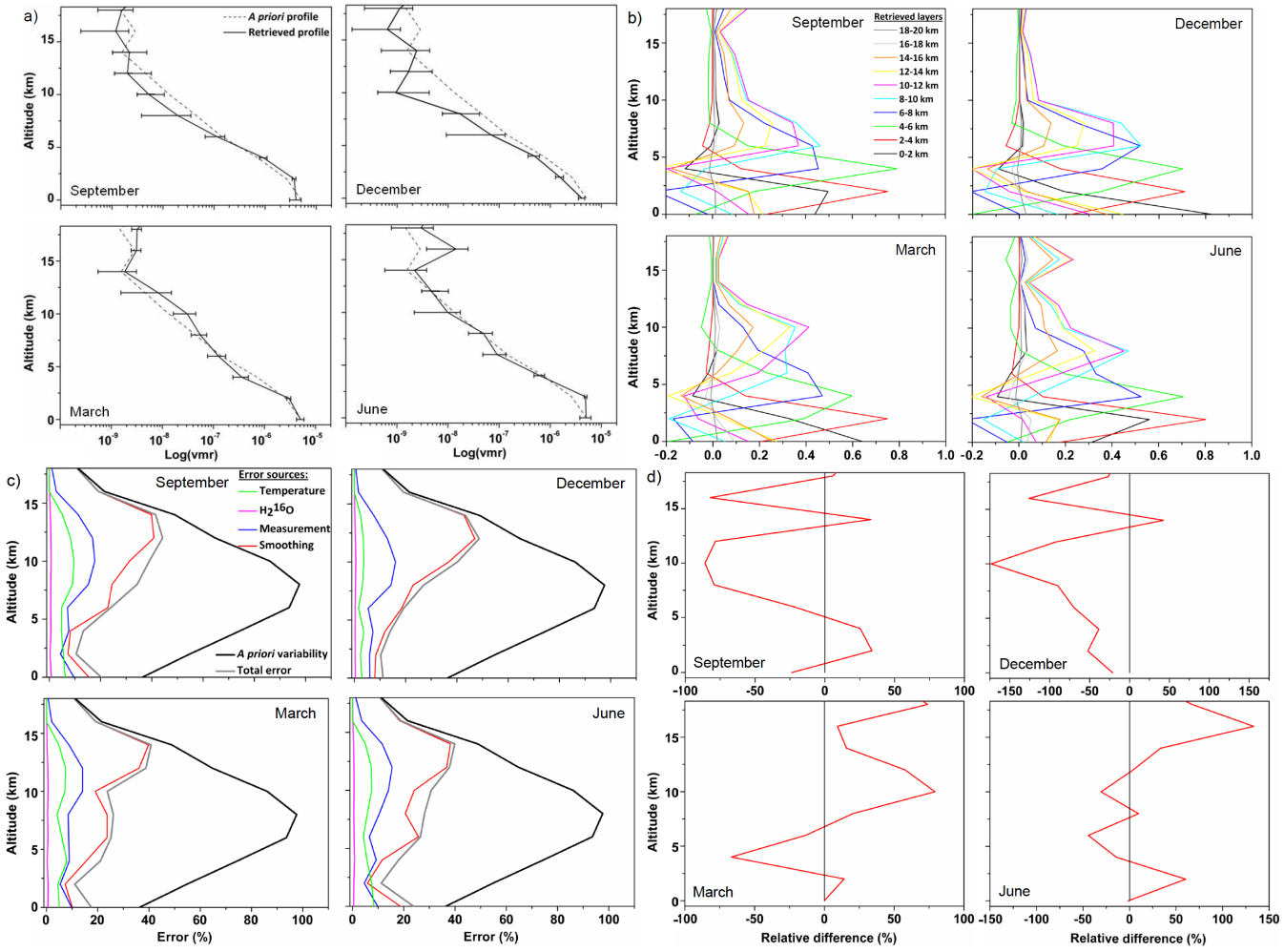

Fig. 7. (a) Same as Fig. 5a for HDO profiles (vmr) retrieved from IASI observations at Hawaii on four days (top to bottom): 21 September 2008, 21 December 2007, 28 March 2008 and 21 June 2008. **(b)** Averaging kernels related to (a), in volume mixing ratio units, for each retrieved layers. The corresponding degrees of freedom for signal are reported in Table 3. **(c)** Error profiles related to (a). **(d)** Relative difference between retrieved and a priori profiles related to (a).

4 Case study

In the previous section we have demonstrated that IASI spectra contain significant information on the distributions of $H_2^{16}O$ and HDO. This opens the perspective for studying atmospheric dynamical and meteorological events, which were not accessible from space borne observations before. In order to illustrate this, we have chosen to perform a preliminary study of the δ_D partitioning on a regional scale, during a typhoon, which is accompanied by extreme and complex hydrologic processes. Water vapour isotopologic ratio measurements act as tracers providing information on cyclones, storms and hurricanes, like structure, evolution, microphysics or water budget (Gedzelman et al., 2003; Lawrence et al., 2003). Unfortunately these measurements are generally limited to rain and vapour collected at the surface or during flights (Lawrence et al., 1996, 1998, 2002, 2003; Gedzelman et al., 2003).

The Krosa typhoon, which was one of the major events of the year 2007, is taken as a case study. The sequence of the typhoon was as follows; it initially formed on 1 October as a tropical depression South-East of the Philippines. Rapid intensification took place and the depression was upgraded to a tropical storm and later to a typhoon. As it intensified, it gained a wide eye and moved North-West, becoming a super typhoon on 5 October when it approached Taiwan. It slowly weakened afterwards before making landfall in Taiwan and South-East China. The sequence is considered to have ended three days later, on 8 October, above the Philippine Sea.

For the retrievals of the isopologues during the 8 days of this event, we have selected cloud free spectra. Only scenes showing a degree of homogeneity larger than 90% have been

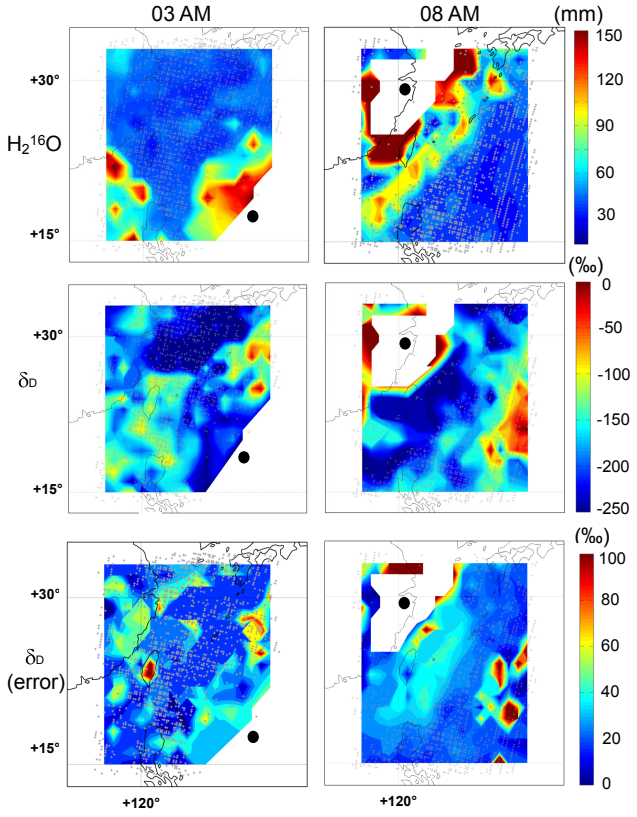

Fig. 8. Distribution of $H_2^{16}O$, δ_D and δ_D error for the mornings of the 3 and 8 October 2007. $H_2^{16}O$ distributions are given as partial columns (0–8 km) in mm. δ_D and δ_D error distributions are in ‰unit averaged on the (0–8 km) partial column. Data are averaged on a $1°\times1°$ longitude-latitude grid. The grey crosses show the location of the IASI retrievals. The full black circles show the location of the typhoon's eye and the white zones identify the cloudy areas.

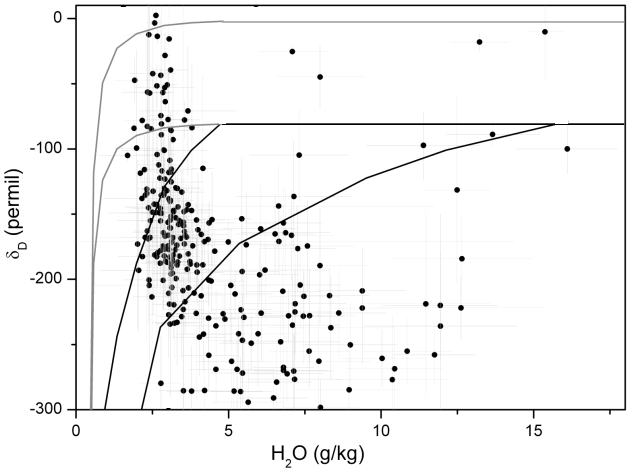

Fig. 9. δ_D (‰) as a function of $H_2^{16}O$ (g/kg) for the 8 October 2007 during Krosa typhoon overpass in South-East Asia. The full black circles show the morning data averaged on a $1°\times1°$ longitude-latitude grid and the light grey crosses are their uncertainties associated The black lines represent the Rayleigh distillation curves with surface temperatures of 288 K (left line) and 300 K (right line), initialized to the surface layer δ_D value of −79‰. The grey lines represent evaporation lines initialized respectively from the same value of δ_D (−79‰) (lower grey line) and the average seasonal δ_D value in regional precipitation (based on Global Network of Isotopes in Precipitation (GNIP) observation).

kept, thus removing cloudy spectra just above and around the typhoon's eye. The resulting distributions, presented in Fig. 8 are averages on a 1° latitude by 1° longitude grid and the unit is in precipitable water vapour (mm). The full black circles in Fig. 8 show the location of the typhoon's eye and the white zones identify the cloudy areas. We focus hereafter on the tropospheric distributions $H_2^{16}O$, δ_D and δ_D error expressed as an integrated column from 0 to 8 km such as to use the vertical range where each species is more sensitive. Moreover, the partial columns avoid comparing profiles with different vertical resolution and averaging reduces the random measurement error. The retrieved $H_2^{16}O$ map for 3 October, reveals two moist fronts: one in the South-East linked to the typhoon's approach, and one above the Philippines corresponding to the end of the tropical storm Lekima which occurred in that region 27 September to 5 October. On 8 October, the map shows again two moist fronts but now in the North-West, the one closest to the typhoon's eye being more important. The quantity of precipitable water is very high near the depression (around 150 mm), but these values are consistent with the heavy rain recorded by the Tropical Rainfall Measuring Mission (TRMM, http://trmm.gsfc.nasa.gov/) satellite (>50 mm per hour and locally 300 mm in few hours). The average δD uncertainty for this distribution is 34‰(bottom panel of Fig. 8), slightly larger when the δD is high. These errors are well below the observed variations in δD surrounding the typhoon (middle panel): On 3 October, the δD are homogeneous, around −125 permil in front of the typhoon, slightly lower closer to its center. On 8 October, the value of δD is high around the eye (close to 0 or positive) but we observe strong depletion at the back after the typhoon has passed (down to −300‰). One further observes that the δ_D map for 3 October does not reveal particular features when compared to the $H_2^{16}O$ distribution, whereas there is on the contrary, except closer the eye, an anti-correlation between δ_D and $H_2^{16}O$ on 8 October (ie or the regions where δ_D values are very low the humidity tends to be very high), likely pointing to an intense depletion in the deuterated isotopologue after the typhoon passed.

To further highlight this, Fig. 9 shows δ_D values as a function of the relative humidity for 8 October. Full circles represent data average on a 1° latitude by 1° longitude grid to be compared with the Fig. 8 and the light grey vertical lines are the associated uncertainties. Rayleigh distillation curves originating from air parcels with saturation specific humidity values based on oceanic temperatures of 288 and 300 K,

and initial δ_D values of $-79‰$(vapour equilibrium with the ocean) are shown as black lines. The grey lines represent the enriching effects that arise from mixing moist marine with drier air parcels. These curves are based on typical tropical surface temperature of 288 K (for more details, see supplemental material of Worden et al., 2007). The Rayleigh distillation curves are commonly used to describe changes in the water isotopic composition. The latter assumes that water is removed as precipitation condenses and fractionation of isotopologic ratios takes place at the thermodynamic equilibrium. This model allows accurate description of many meteorological events like tropical cyclones (Gedzelman et al., 1982), but it is less accurate when the hydrometeors and water vapour interactions become important. In these cases the Rayleigh distillation curves are reference to determine the history of evaporation and condensation processes.

The large variability of the retrieved δ_D values suggests important mixing processes, including turbulent transport and large scale advection over the analyzed region. 46% of the measurements are constrained by Rayleigh distillation lines and 19% by evaporation lines: These cases correspond in particular to the South-Eastern measurements of Fig. 8 in a location far from the typhoon where the air is dryer after the typhoon has crossed. In contrast many points (27%) are more depleted than predicted by the Rayleigh distillation model especially near the rain bands (North-West of Fig. 8). This is an example of the "amount effect" (Dansgaard, 1964), in which isotopologic ratios are negatively correlated with total water amounts.

The typical δ_D uncertainties for vertically averaged values that we obtain are low enough to not affect the discussion of these distributions, nevertheless they point towards the limitations of our δ_D calculation approach for such analyses. Likewise, to go further in the meteorological events, and in particular typhoon understanding it is necessary to improve the retrieval of cloudy spectra. This will allow for instance having water vapour profiles closer to the eye and so obtain information about typhoon dynamic.

5 Conclusions

A set of high-resolution Fourier transform nadir spectra measured by the IASI instrument have been analyzed to obtain vertical tropospheric distributions of two isotopologic species of water vapour ($H_2^{16}O$ and HDO). The retrievals were made using software relying on the OEM, allowing to measure volume mixing ratios and partial columns from the ground up to 20 km; the retrievals were performed simultaneously for both species but without putting a correlation constrain between them. The measurements contain up to 6 ($H_2^{16}O$) and 3.5 (HDO) independent pieces of information on the vertical distributions, with the sensitivity of IASI being highest between the surface and 8 km. At these altitudes, the theoretical uncertainties are less than 15% on each retrieved level of the profile for the principal isotopologue and 25% for HDO for low and mid-latitudes, independently of the season. The uncertainties are larger at high latitudes because of the lower humidity and spectral radiances. We have found, however, that the theoretical uncertainties, which comply with the mission objectives, were difficult to achieve in reality. Indeed, the comparison of the retrieved profiles with coincident sonde measurements, performed at a series of representative latitudes and seasons, shows the potential of IASI to capture the large-scale spatial variations of water vapour in the troposphere but with errors that can be as large as 50% at several levels of the profile in the free and the upper troposphere. An important result from the sensitivity studies conducted in this work is to demonstrate the gain of information on the surface HDO retrievals using the solar reflected part of spectra during daytime. Another key aspect is the quantification of the δ_D calculated from the individual profile retrievals and of its associated error, which enables geophysical studies to be carried out provided sufficient vertical averaging is performed.

The $H_2^{16}O$ and δ_D zonal distributions of partial columns above South-East Asia during a major meteorological event (Krosa super typhoon) have been studied on these grounds. Significant and meaningful horizontal variations of the δ_D values during the Typhoon sequence are found, and in particular a very high depletion of the δ_D values after the typhoon crossing has been observed, producing the so-called amount effect. The analysis of δ_D as a function of H_2O for that event has revealed that about one third of the measurements are not following the Rayleigh model, thus allowing for a distinction between evaporation and condensation processes. These encouraging and original results concern only the cloudy free spectra, that is to say relatively far from the typhoon's eye. In the future it would be important to improve the retrievals of the cloudy spectra in order to better study the typhoon's dynamic.

Globally, the results have demonstrated the ability of the IASI instrument to measure $H_2^{16}O$ and HDO profiles accurately and with a good coverage and sampling. These results open promising perspectives for measuring δ_D profiles and then analyses of meteorological processes on extended spatial scales and over longer periods. Finally, interesting information on $H_2^{18}O$ is obtained as well, with 3 to 4 degrees of freedom for signal (DOFS), but the characterization of this isotopologue is more challenging; it was therefore not discussed here, but it will be the aim of a future study.

Acknowledgements. IASI has been developed and built under the responsibility of the Centre National d'Etudes Spatiales (CNES, France). It is flown onboard the Metop satellites as part of the EUMETSAT Polar System. The IASI L1 data are received through the EUMETCast near real time data distribution service. The research in Belgium was funded by the F. R. S.-FNRS (M. I. S. nF.4511.08), the Belgian State Federal Office for Scientific, Technical and Cultural Affairs and the European Space Agency (ESA-Prodex arrangements C90-327). Financial support by the "Communauté française de Belgique – Actions de Recherche Concertées" is also acknowledged. C. Clerbaux acknowledges CNES for the financial support.

Edited by: A. Richter

References

Barret, B., Turquety, S., Hurtmans, D., Clerbaux, C., Hadji-Lazaro, J., Bey, I., Auvray, M., and Coheur, P.-F.: Global carbon monoxide vertical distributions from spaceborne high-resolution FTIR nadir measurements, Atmos. Chem. Phys., 5, 2901–2914, 2005, http://www.atmos-chem-phys.net/5/2901/2005/.

Beer, R., Glavich, T. A., and Rider, D. M.: Tropospheric emission spectrometer for the Earth Observing System's Aura Satellite, Appl. Optics, 40(15), 2356–2367, 2001.

Bowen, G. J. and Revenaugh, J.: Interpolating the isotopologic composition of modern meteoric precipitation, Water Resour. Res., 39(9), 1299, doi:2003WR002086, 2003.

Brown, D., Worden, J., and Noone, D.: Comparison of hydrology over convective continental regions using water vapor isotope measurements from space, J. Geophys. Res., 113, D15124, doi:10.1029/2007JD009676, 2008.

Ciais, P. and Jouzel, J.: Deuterium and oxygen 18 in precipitation: Isotopologic model, including mixed cloud processes, J. Geophys. Res., 99(D8), 16793, doi:94JD00412, 1994.

Clerbaux, C., Hadji-Lazaro, J., Turquety, S., George, M., Coheur, P.-F., Hurtmans, D., Wespes, C., Herbin, H., Blumstein, D., Tournier, B., and Phulpin, T.: The IASI/MetOp mission: first observations and highlight of its potential contribution to the GMES Earth observation component, Space Res. Today, 168, 19–24, 2007.

Clerbaux, C., Boynard, A., Clarisse, L., George, M., Hadji-Lazaro, J., Herbin, H., Hurtmans, D., Pommier, M., Razavi, A., Turquety, S., Wespes, C., and Coheur, P.-F.: Monitoring of atmospheric composition using the thermal infrared IASI/MetOp sounder, Atmos. Chem. Phys., 9, 6041–6054, 2009, http://www.atmos-chem-phys.net/9/6041/2009/.

Coffey, M. T., Hannigan, J. W., and Goldman, A.: Observations of upper tropospheric/lower stratospheric water vapour and its isotopologues, J. Geophys. Res., 111, D14, doi:10.1029/2005JD006093, 2006.

Coheur, P.-F., Barret, B., Turquety, S., Hurtmans, D., Hadji-Lazaro, J., and Clerbaux, C.: Retrieval and characterization of ozone vertical profiles from a thermal infrared nadir sounder, J. Geophys. Res., 110, D24, doi:2005JD005845, 2005.

Dansgaard, W.: Stable isotopes in precipitation, Tellus, 16(3), 436–468, 1964.

Ehhalt, D. H., Rohrer, F., and Fried, A.: Vertical profiles of HDO/H_2O in the troposphere, J. Geophys. Res., 110, D13, doi:10.1029/2004JD005569, 2005.

Franz, P. and Rckmann, T.: High-precision isotope measurements of $H_2^{16}O$, $H_2^{17}O$, $H_2^{18}O$, and the $\Delta^{17}O$-anomaly of water vapor in the southern lowermost stratosphere, Atmos. Chem. Phys., 5, 2949–2959, 2005, http://www.atmos-chem-phys.net/5/2949/2005/.

Gaffen, D.: Temporal inhomogeneities in radiosonde temperature records, J. Geophys. Res., 99D2, 3667–3676, 1994.

Galewsky, J., Strong, M., and Sharp, Z. D.: Measurements of water vapor D/H ratios from Mauna Kea, Hawaii, and implications for subtropical humidity dynamics, Geophys. Res. Lett., 34, L22808, doi:10.1029/2007GL031330, 2007.

Gedzelman, S. D. and Lawrence, J. R.: The isotopic composition of cyclonic precipitation, J. Appl. Meteorol., 21, 1385–1404, 1982.

Gedzelman, S. D., Hindman, E., Zhang, X., Lawrence, J., Gamache, J., Black, M., Black, R., Dunion, J., and Willoughby, H.: Probing Hurricanes with stable isotopologues of rain and water vapor, Mon. Weather Rev., 131, 1112–1127, 2003.

Gettelman, A. and Webster, C. R.: Simulations of water isotopologue abundances in the upper troposphere and lower stratosphere and implications for stratosphere troposphere exchange, J. Geophys. Res., 110, D17, doi:10.1029/2004JD004812, 2005.

Hanisco, T. F., Moyer, E. J., Weinstock, E. M., St. Clair, J. M., Sayres, D. S., Smith, J. B., Lockwood, R., and Anderson, J. G.: Observations of deep convective influence on stratospheric water vapor and its isotopic composition, Geophys. Res. Lett., 34, L048141–L048145, 2007.

Hartmann, D. L.: Climate Change: Tropical Surprises, Science, 295, 811–812, 2002.

Herbin, H., Hurtmans, D., Turquety, S., Wespes, C., Barret, B., Hadji-Lazaro, J., Clerbaux, C., and Coheur, P.-F.: Global distributions of water vapour isotopologues retrieved from IMG/ADEOS data, Atmos. Chem. Phys., 7, 3957–3968, 2007, http://www.atmos-chem-phys.net/7/3957/2007/.

Johnson, D. J., Jucks, K. W., Traub, W. A., and Chance, K. V.: Isotopic composition of stratospheric water vapor: Implications for transport, J. Geophys. Res., 106(D11), 12219–12226, 2001.

Kuang, Z. M., Toon, G. C., Wennberg, P. O., and Yung, Y. L.: Measured HDO/H_2O ratios across the tropical tropopause, Geophys. Res. Lett., 30(6), 1372, doi:2003GL017023, 2003.

Lawrence, J. R. and Gedzelman, S. D.: Low stable isotope ratios of tropical cyclone rains, Geophys. Res. Lett., 23(4), 527–530, 1996.

Lawrence, J. R., Gedzelman, S. D., Zhang, X., and Arnold, R.: Stable isotope ratios of rain and vapor in 1995 hurricanes, J. Geophys. Res., 103(9), 11381–11400, 1998.

Lawrence, J. R., Gedzelman, S. D., Gamache, J., and Black, M.: Stable isotopologue ratios: Hurricane Olivia, J. Atmos. Chem., 41, 67–82, 2002.

Lawrence, J. R., and Gedzelman, S. D.: Tropical ice core isotopes: Do they reflect changes in storm activity, Geophys. Res. Lett., 30(2), doi:10.1029/2002GL015906, 2003.

McCarthy, M. C., Boering, K. A., Rahn, T., Eiler, J. M., Rice, A. L., Tyler, S. C., Schauffler, S., Atlas, E., and Johnson, D. G.: The hydrogen isotopologic composition of water vapour entering the stratosphere inferred from high-precision measurements of δ_D-CH_4 and δ_D-H_2, J. Geophys. Res., 109, D07, doi:10.1029/2003JD004003, 2004.

Moyer, E. J., Irion, R. W., Yung, Y. L., and Gunson, M. R.: ATMOS stratospheric deuterated water vapour and implications for troposphere-stratosphere transport, Geophys. Res. Lett., 23(17), 2385, doi:96GL01489, 1996.

Razavi, A., Clerbaux, C., Wespes, C., Clarisse, L., Hurtmans, D., Payan, S., Camy-Peyret, C., and Coheur, P. F.: Characterization of methane retrievals from the IASI space-borne sounder, Atmos. Chem. Phys., 9, 7889–7899, 2009, http://www.atmos-chem-phys.net/9/7889/2009/.

Rodgers, C. D.: Inverse Methods for Atmospheric Sounding: Theory and Practice, World Sci., Hackensack, N. J., 2000.

Rosenlof, K. H., Oltmans, S. J., Kley, D., Russell, J. M., Chiou, E.-W., Chu, W. P., Johnson, D. G., Kelly, K. K., Michelsen, H. A., Nedoluha, G. E., Remsberg, E. E., Toon, G. C., McCormick, M. P.: Stratospheric water vapour increases over the past half-century, Geophys. Res. Lett., 28(6), 1195, doi:2000GL012502, 2001.

Rosenlof, K. H.: How water enters the stratosphere, Science, 302, 1691–1692, 2003.

Rothman, L. S., Jacquemart, D., Barbe, A., et al.: The HITRAN 2004 molecular spectroscopic database, J. Quant. Spectrosc. Ra., 96, 139–204, 2005.

Schlüssel, P., Hultberg, T. H., Phillips, P. L., August, T., and Calbet, X.: The operational IASI Level 2 processor, Adv. Space Res., 36, 982–988, 2005.

Schmidt, G. A., Hoffmann, G., Shindell, D. T., and Hu, Y.: Modelling atmospheric stable water isotopologues and the potential for constraining cloud processes and stratosphere-troposphere water exchange, J. Geophys. Res., 110, D21, doi:2005JD005790, 2005.

Schneider, E. K., Kirtman, B. P., and Lindzen, R. S.: Tropospheric Water Vapour and Climate Sensitivity, J. Atmos. Sci., 56, 1649–1658, 1999.

Schneider, M., Hase, F., and Blumenstock, T.: Ground-based remote sensing of HDO/H_2O ratio profiles: introduction and validation of an innovative retrieval approach, Atmos. Chem. Phys., 6, 4705–4722, 2006, http://www.atmos-chem-phys.net/6/4705/2006/.

Smith, R. B.: Deuterium in North Atlantic storm tops, J. Atmos. Sci., 49, 2041–2057, 1992.

Steinwagner, J., Milz, M., von Clarmann, T., Glatthor, N., Grabowski, U., Höpfner, M., Stiller, G. P., and Röckmann, T.: HDO measurements with MIPAS, Atmos. Chem. Phys., 7, 2601–2615, 2007, http://www.atmos-chem-phys.net/7/2601/2007/.

Strong, M., Scharp, Z. D., and Gutzler, D. S.: Diagnosing moisture transport using D/H ratios of water vapor, Geophys. Res. Lett., 34, L03404, doi:2006GL028307, 2007.

University of Wyoming' department of atmospheric sciences radiosondes data base: http://weather.uwyo.edu/upperair/sounding.html.

Webster, C. R. and Heymsfield, A. J.: Water isotopologue ratios D/H, $^{18}O/^{16}O$, $^{17}O/^{16}O$ in and out of clouds map dehydration pathways, Science, 302, 1742–1745, 2003.

Worden, J., Bowman, K., Noone, D., et al.:: Tropospheric Emission Spectrometer observations of the tropospheric HDO/H_2O ratio: Estimation approach and characterization, J. Geophys. Res., 111, D16, doi:10.1029/2005JD006606, 2006.

Worden, J., Noone, D., Bowman, K., et al.: Importance of rain evaporation and terrestrial sources in the tropical water cycle, Nature, 445, 528–553, 2007.

Zahn, A., Franz, P., Bechtel, C., Grooß, J.-U., and Röckmann, T.: Modelling the budget of middle atmospheric water vapour isotopes, Atmos. Chem. Phys., 6, 2073–2090, 2006, http://www.atmos-chem-phys.net/6/2073/2006/.

Zhang, X., Tian, L., and Liu, J.: Fractionation mechanism of stable isotope in evaporating water body, J. Geophys. Res., 15, 375–384, 2005.